

Supporting Information for

The *para*-fluoro-thiol reaction as a powerful tool for precision network synthesis

Federica Cavalli,¹ Hatice Mutlu,^{1,2} Sven O. Steinmueller,³ Leonie Barner,^{1,4}*

¹ Soft Matter Synthesis Laboratory, Institut für Biologische Grenzflächen, Karlsruhe Institute of Technology (KIT), Hermann-von-Helmholtz-Platz 1, 76344, Eggenstein-Leopoldshafen, Germany

² Macromolecular Architectures, Institut für Technische Chemie und Polymerchemie, Karlsruhe Institute of Technology (KIT), Engesserstraße 18, 76128 Karlsruhe, Germany

³ Surface Analysis Group, Institute for Applied Materials, Karlsruhe Institute of Technology (KIT), Hermann-von-Helmholtz-Platz 1, 76344, Eggenstein-Leopoldshafen, Germany

⁴ School of Chemistry, Physics and Mechanical Engineering and Institute of the Future Environments, Queensland University of Technology (QUT), 2 George Street, QLD 4000, Brisbane, Australia
e-mail: leonie.barner@qut.edu.au

Content:

A. Experimental procedure

A.1. Materials

A.2. Characterization Methods and Equipment

A.2.1. Nuclear Magnetic Resonance (NMR) Spectroscopy

A.2.2. Size Exclusion Chromatography (SEC)

A.2.3. Electrospray Ionization Mass Spectrometry (ESI-MS)

A.2.4. Attenuated Total Reflectance - Infrared Spectroscopy (ATR-IR)

A.2.5. X-Ray Photo electron Spectroscopy (XPS)

A.2.6. Time-of-Flight Secondary Ion Mass Spectrometry (ToF-SIMS)

A.2.7. Differential Scanning Calorimetry (DSC)

A.3. Regioselectivity of the *para*-fluoro thiol ligation

A.4. Synthesis of the fluorinated linker (3PFB)

A.5. General procedure for the “Model Reaction 3+1”

A.6. General procedure for network formation

B. References

A – Experimental Procedure

A1 - Materials

1,1,1-tris(hydroxymethyl)ethane (99%, Sigma Aldrich), 2,3,4,5,6-pentafluorobenzyl bromide (98%, Alfa Aesar), sodium hydroxide (NaOH, $\geq 99\%$, Roth), tetrabutylammonium bromide (99%, ABCR), 1-dodecanethiol (DDT, 98%, ABCR), 1,4-phenylenedimethanethiol (PDT, $>98\%$, TCI), 1,4-butanedithiol (BT, $>95\%$, TCI), 3,6-dioxa-1,8-octanedithiol (DODT, 95%, Sigma Aldrich), dithiothreitol (DTT, molecular biology grade, AppliChem), 1,8-diazabicyclo[5.4.0]undec-7-ene (DBU, 98 %, Sigma Aldrich), benzoic acid (BA, $\geq 99.5\%$, Alfa Aesar), sodium chloride (NaCl, 99.9%, AnalR NORMAPUR), magnesium sulfide (Mg_2SO_4 , 99.5%, Alfa Aesar) dichloromethane (DCM, 99.8%, AnalR NORMAPUR), tetrahydrofuran (THF, HiPerSolv CHROMANORM, stabilized with BHT, VWR), cyclohexane (CycloHex, $>99.5\%$, AnalR NORMAPUR), ethanol (99.8%, AnalR NORMAPUR). Deuterated solvents: chloroform-*d* (CDCl_3 , $>99.9\%$), tetrahydrofuran-*d8* (THF-*d8*, $>99.5\%$) were purchased from Euriso-Top. All the chemicals and solvents were used without further purification.

A.2 - Characterization Methods and Equipment

A.2.1 Nuclear Magnetic Resonance (NMR) Spectroscopy: ^1H -, ^{13}C - and ^{19}F -NMR measurements were carried out using a Bruker Avance III 400 spectrometer (^1H , 400 MHz; ^{13}C , 100 MHz; ^{19}F , 376 MHz). For cross-linked material, the product was placed in the NMR tube and swollen in CDCl_3 . Thereafter, the NMR data was recorded following the common procedure as for the liquid samples; all other analytes were dissolved in CDCl_3 prior to recording the spectrum. The residual solvent signals were employed for shift correction (for ^1H -NMR spectra at 7.26 ppm, for ^{13}C -NMR at 77.16 ppm). For the ^{19}F -NMR spectra, the following corrections were made: baseline correction with the Bernstein polynomial fit (with a polynomial order of 20) and manual correction. Abbreviations used in the compound description include singlet (s), doublet (d), triplet (t), multiplet (m) and their combinations.

A.2.2. Size Exclusion Chromatography (SEC) traces were recorded using a TOSOH Eco-SEC HLC-8320 GPC System, comprising an auto sampler, a SDV 5 μm bead-size guard column (50 x 8 mm, PSS) followed by three SDV 5 μm columns (300 x 7.5 mm, subsequently 100 \AA , 1000 \AA and 10^5 \AA pore size, PSS), a differential refractive index (DRI) detector and an UV detector. Tetrahydrofuran was used as eluent at 30 $^\circ\text{C}$ with a flow rate of 1 mL min^{-1} . The SEC system was calibrated using linear polystyrene (PS) standards ranging from 266 to $2.52 \cdot 10^6$ g mol^{-1} . Calculation of the molecular weight proceeded via the Mark-Houwink-Sakurada (MHS) parameters in THF at 30 $^\circ\text{C}$, $K = 13.63 \cdot 10^{-3} \text{ mL g}^{-1}$, $\alpha = 0.714$.

A.2.3. Electrospray Ionization Mass Spectrometry (ESI-MS) was performed on a Q Exactive (Orbitrap) mass spectrometer (Thermo Fisher Scientific, San Jose, CA, USA) equipped with a HESI II probe. The instrument calibration was carried out in the m/z range 74 – 1822 using calibration solutions from Thermo Scientific. A constant spray voltage of 3.6 kV and a dimensionless sheath gas of 5 were applied. The capillary temperature and the S-lens RF level were set to 320 $^\circ\text{C}$ and 62.0 $^\circ\text{C}$, respectively. The samples were dissolved in a THF:MeOH (3:2) mixture containing 100 μmol of sodium triflate and injected with a flow of 5 $\mu\text{L}\cdot\text{min}^{-1}$.

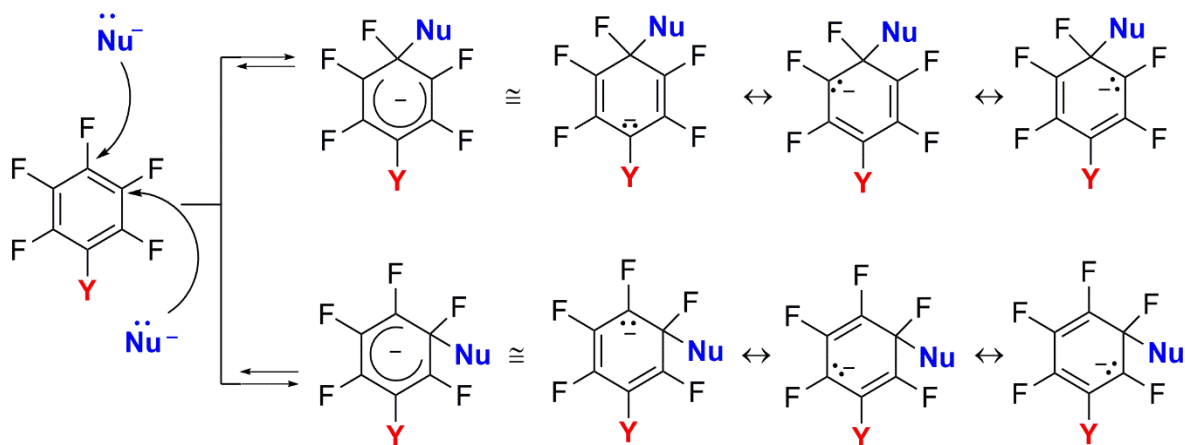
A.2.4. Attenuated Total Reflectance - Infrared Spectroscopy (ATR-IR) – Bruker Vertex 80 Solid-state Fourier transform IR spectra were recorded using a Bruker Vertex 80 spectrometer, equipped with a tungsten halogen lamp, a KBr beam splitter, and a DTGS detector.

A.2.5. X-Ray Photo electron Spectroscopy (XPS) was performed with a K-Alpha+ XPS instrument (Thermo Fisher Scientific, East Grinstead, England). At least three random points for each sample were analysed using a microfocused, monochromated Al K α X-ray source (400 μm spot size) The K-Alpha+ charge compensation system was employed during analysis, using electrons of 8 eV energy and low-energy argon ions to prevent any localized charge build-up. Spectra were fitted with several Voigt profiles (binding energy uncertainty of \pm 0.1 eV). The analyzer transmission function, Scofield sensitivity factors¹ and effective attenuation lengths (EALs) for photoelectrons were applied for quantification. EALs were calculated using the standard TPP-2M formalism.² All spectra were referenced to the C1s peak (C-C, C-H) at 285.0 eV binding energy controlled by the means of the well-known photoelectron peaks of metallic Cu, Ag and Au.

A.2.6. Time-of-Flight Secondary Ion Mass Spectrometry (ToF-SIMS) was recorded using a ToF-SIMS 5 instrument (ION-TOF GmbH, Muenster, Germany). Surface spectroscopy was carried out with Bi₃⁺ as primary ion for secondary ion generation. Measurements were performed on two different positions of each sample obtaining surface images with high mass resolution. Surface charging was avoided by compensation with a low energy (<20 eV) electron beam. The recorded data was flight time corrected using the Advanced ToF Correction feature of the SurfaceLab 6.6 software of the instrument. All images show a recorded area of 500 x 500 μm with 128 x 128 data points obtaining a resolution of about 4 μm per measurement point. Images are normalized to the total ion intensity. Brighter colours indicate higher intensity values. Colour scales of specific fragments have always the same values.

A.2.7. Different Scanning Calorimetry (DSC) experiments were carried out under nitrogen atmosphere using 40 μL aluminium crucibles with a DSC821e (Mettler Toledo) calorimeter, using sample mass in the range of 8–15 mg. For analysis the following method was employed: the first heating proceeded from -75 °C to 300 °C at a heating rate of 10 °C min⁻¹; a cooling step was performed from 300 °C to -75 °C at a heating rate of 10 °C; the second heating run was recorded from -75 °C to 300 °C at a heating rate of 10 °C min⁻¹. The glass transition temperature, T_g , is reported as the midpoint of the heat capacity change in the first heating scan.

A.3 – Regioselectivity of *Para*-fluoro-thiol Ligation



Scheme 1. Resonance structures for the nucleophilic substitution of fluorine atoms in monosubstituted aromatic ring⁴ (Y refers in this work to the core of the linker (3PFB)).

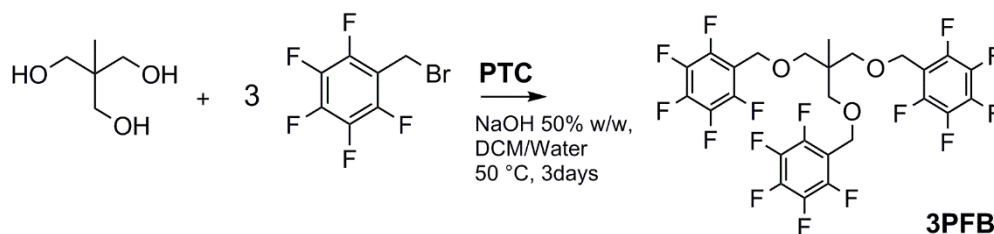
The *para*-fluoro-thiol reaction (PTFR) employed for network formation is part of the family of nucleophilic substitution reactions. In the current work, a bifunctional thiol acts as a nucleophilic agent attaching to the pentafluorobenzyl moieties (PFB). However, before moving towards more complicated routes such as network formation, an insight into the regioselectivity of the reaction is fundamental. In detail, the three armed linker (3PFB) mentioned in the main text can be considered as a particular example of monosubstituted pentafluorobenzenes, where the core of the linker itself is represented by the letter Y in Scheme 1.

As explained by Louis Plank Hammet in 1937,³ and now well-known in the field of aromatic chemistry, when the aromatic system exhibits a substituent, the regioselectivity is regulated by the nature of the substituent itself. The regioselectivity is explained by the Hammett equation, which general formula is:

$$\log \frac{K}{K_0} = \sigma \rho$$

Where K is the equilibrium constant of a given reaction performed with a general substituent R and K_0 refers to the same reaction where R is a hydrogen atom. Correspondingly, σ depends on the specific substituent R (substituent constant) and ρ is determined only by the type of reaction itself (reaction constant). The substituent constant can be determined for each position of the aromatic ring and their values define the so called “effect of the substituent” which drives the regioselectivity of the reaction. In this specific case, the substituent Y is located in *para* position with respect to the position in which the PTFR is expected to occur. Therefore, the main parameter of interest is the *para*-substituent constant (σ_p). As shown in Scheme 1, the *para*-substitution is promoted by the pathway proposed in the upper line. These mesomeric resonance structures, as recently reported by Kvičala *et al.*, are destabilized by substituents Y with σ_p value below -0.20 (which will instead promote the *meta*-substitution) and stabilized by substituents with a positive value of σ_p .⁴ Hence, in the current work, in order to selectively promote the *para*-substitution, an aliphatic ether core was chosen, where $Y = -\text{CH}_2\text{O}$ which is characterized by a σ_p of 0.02.⁵

A.4 - Synthesis of the Fluorinated Linker Trimethylolpropane tris(2,3,4,5,6-pentafluorobenzylether) (3PFB)



Scheme 2. Schematic synthetic route of trimethylolpropane tris(2,3,4,5,6-pentafluorobenzylether) (**3PFB**) obtained via Phase Transfer Catalysis (PTC).

To a stirred aqueous solution of sodium hydroxide (90.0 mmol, 3.60 g, 9.0 eq., $C_{\text{NaOH}} = 50 \text{ wt\%}$), 1,1,1-tris(hydroxymethyl)ethane (10.0 mmol, 1.00 g, 1.0 eq) and tetrabutylammonium bromide (TBAB, 0.5 mmol, 0.32 g 0.3 eq., phase transfer catalyst) were added. After stirring at a.t. for 2 h, a solution of 2,3,4,5,6-pentafluorobenzyl bromide (80 mmol, 12 mL, 8.0 eq) in dichloromethane (DCM, $c = 10 \text{ mmol mL}^{-1}$) was added. Subsequently, the temperature was increased to 50 °C, then the reaction mixture was stirred for 3 days. Eventually, the product mixture was cooled to a. t. and washed with water (1x 50 mL), NaOH 0.1 M (2x 50 mL) and brine (1x 50 mL). The aqueous phases were collected and extracted with DCM (1x 100mL). The combined organic layers were dried over Mg_2SO_4 , dried *in vacuo* and subjected to purification on a silica gel column (4:1 CycloHex/DCM) to afford a white crystalline compound (yield 35%).

$^1\text{H NMR}$ (400 MHz, CDCl_3) δ : 0.88 (s, 3H, CH₃), 3.3 (s, 6H, CH₂), 4.54 (s, 6H, CH₂) (Fig.S1).

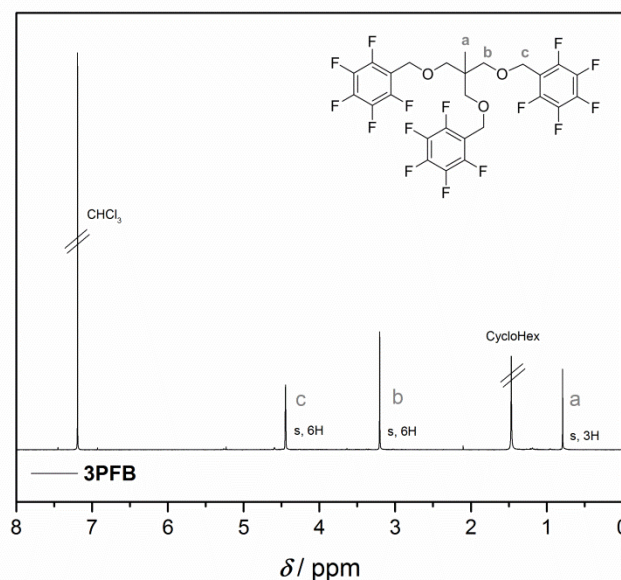


Fig.S1 - $^1\text{H-NMR}$ (400 MHz) spectra of 3PFB in CDCl_3 .

^{13}C NMR (100 MHz, CDCl_3) δ : 17.2 (1C), 40.7 (1C), 60.2 (3C), 72.8 (3C), 111.4 (3C), 136-147 (12C) (Fig. S2).

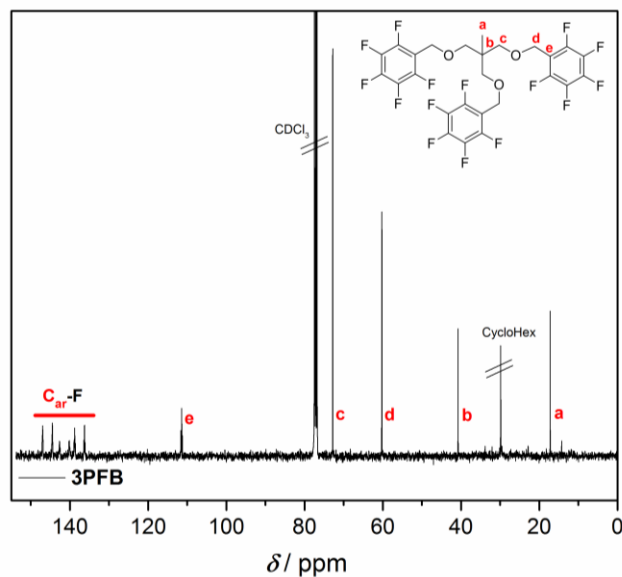


Fig.S2 - ^{13}C -NMR (100 MHz) spectra of 3PFB in CDCl_3 .

^{19}F NMR (376.49 MHz, CDCl_3) δ : -143.2 (dd, 2F, ortho), -153.9 (t, 1F, para), -162 (dt, 2F, meta) (Fig.S3).

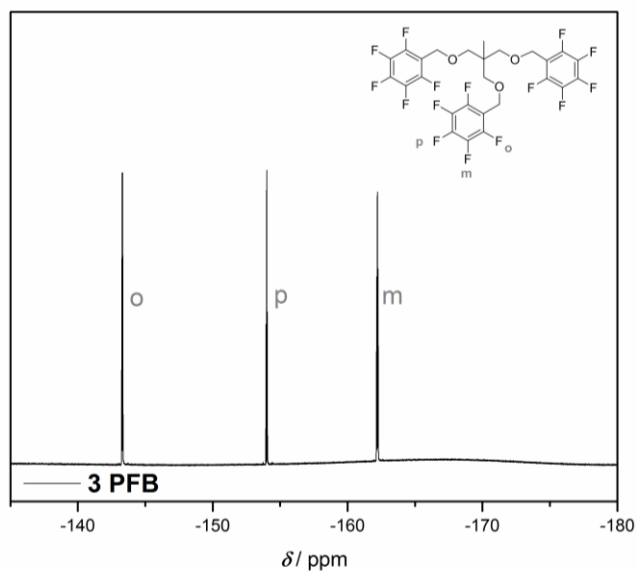
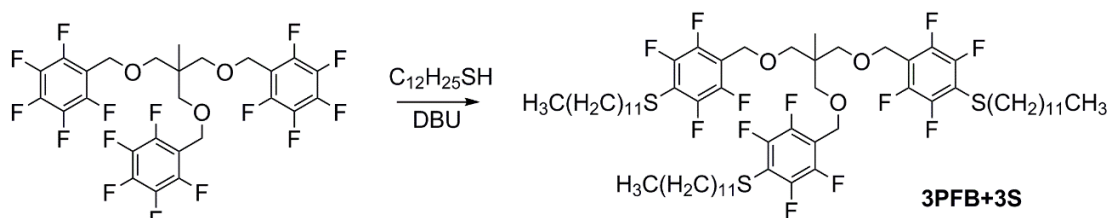


Fig.S3 - ^{19}F -NMR (376.49 MHz) spectra of 3PFB in CDCl_3 .

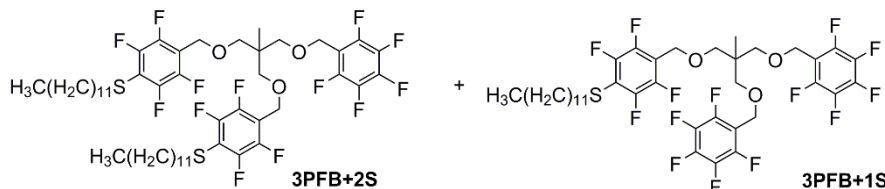
(ESI) m/z : $[\text{3PFB} + \text{Na}]^+$ _{theoretical} 683.0789; $[\text{3PFB} + \text{Na}]^+$ _{experimental} 683.0789.

Melting point (DSC): 58.30 °C

A.5 General Procedure for “Model Reaction 3+1”



Possible by-products:



Scheme 3: Schematic representation of the “Model Reaction 3+1” and possible by-products.

The effects of PFB concentration and time on the reaction rate and reaction products were studied. For the former, reactions applying three concentrations were performed. The concentration of the PFB functionality was selected as $C_{\text{PFB}} = 0.15, 0.30$ and 0.50 M. For the latter, the reaction is stopped at predetermined times (5, 10, 20, 30 and 45 min). In general, a stock solution of DBU ($C_{\text{DBU}} = 4$ M), and dodecanethiol ($C_{\text{SH}} = 3$ M) in THF-d8 were prepared. For these two chemicals, the volumes described in the procedure refer to the volume of stock solution.

The 3PFB linker (0.091 mmol, 0.060 mg, 1 eq.) and dodecanethiol (0.27 mmol, 0.087 mL, 3 eq.) were dissolved in THF-d8 (1.800, 0.900, 0.550 mL, respectively). The reaction mixture was divided in 6 vials and DBU (total amount: 0.27 mmol, 0.068 mL, 3 eq. / each vial: 0.04 mmol, 0.010 mL) was added at a.t. in order to start the reaction, with the exception of one vial representing the time 0. By addition of an excess of benzoic acid (BA) with respect to DBU (4 eq. of BA), the reaction mixture is quenched at prefixed reaction times. Subsequently, a volume corresponding to 2 mg of thiol was withdrawn and used for the SEC analysis in a concentration equal to 2 mg/mL. The peak maxima of the SEC traces at 5 min reaction (Fig. S4) are assigned to the possible reaction products by comparison with the ESI-MS pattern obtained from the same sample (Fig. S5). By these means, the peak maxima of the SEC trace were assigned to 3PFB, 3PFB + 1S (*i.e.* one thiol ligated to 3PFB), 3PFB + 2S (*i.e.* two thiols ligated to 3PFB), and 3PFB + 3S (*i.e.* three thiols ligated to 3PFB). These assignments were used for all other SEC traces as well.

The results from the kinetic are presented in Fig. S6 and S7, where the effect of concentration at fixed time and of time at a fixed concentration is evidenced, respectively. On the other hand, a spectroscopic characterization such as the one arising from NMR spectroscopy is relevant for the identification of the product. In detail, $^1\text{H-NMR}$ and $^{19}\text{F-NMR}$ were recorded. However, despite the GPC traces show the progress of the reaction, the magnetic resonance signals of the adduct in the $^1\text{H-NMR}$ spectra cannot be identified without performing an aqueous work up of the reaction mixture (Fig. S8). After that, one could observe a shift from $\delta=2.68$ ppm to $\delta=2.95$ ppm for the protons in the $\alpha\text{-CH}_2$ to the newly formed S-C_{ar} bond. Furthermore, the resonance of protons belonging to the $\beta\text{-CH}_2$ shifted from $\delta=1.67$ ppm to $\delta=1.56$

ppm (Fig. S8). In agreement with the proposed pathway is also the ^{19}F -NMR already presented and widely discussed in the main text.

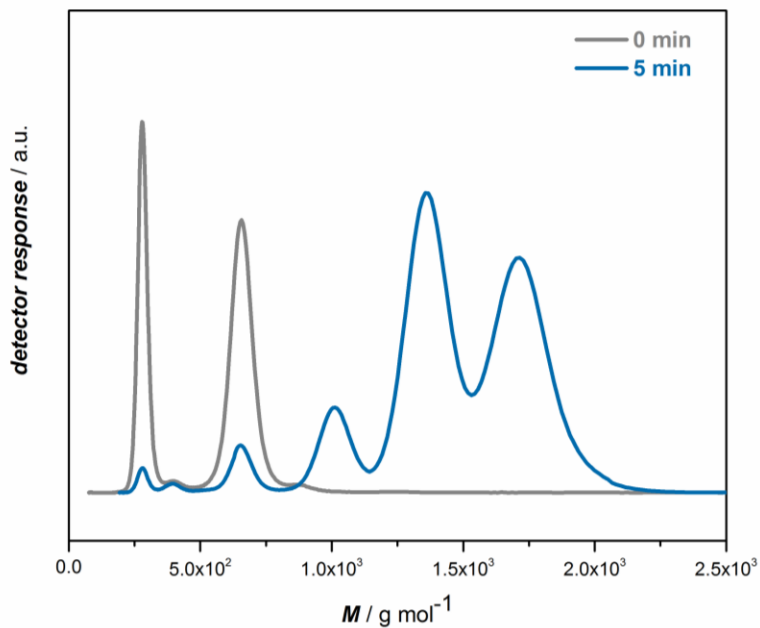


Fig.S4 – Comparison of the SEC traces for $t = 0$ min and $t = 5$ min, where $C_{\text{PFB}} = 0.15$ M.

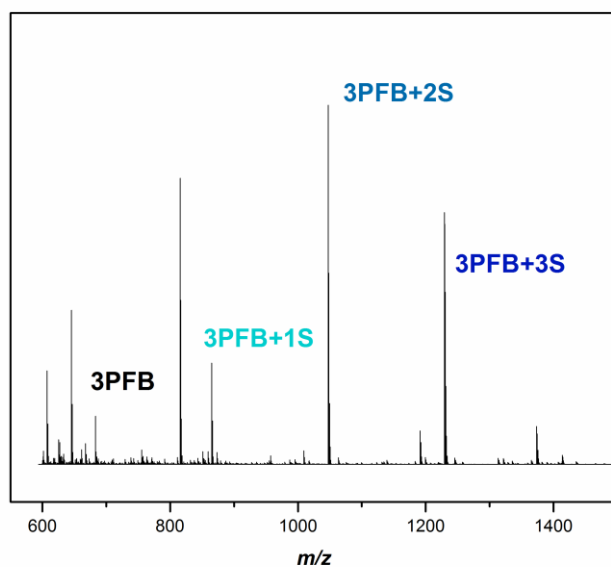


Fig.S5 - High resolution ESI-MS analysis of the same sample employed for GPC analysis (Fig. S4). 3PFB (theo: 683.0681 , exp 683.0681), 3PFB+1S (theo: 865.2367 , exp 865.2377), 3PFB+2S (theo: 1047.4060 , exp 1047.4077), 3PFB+3S (theo: 1229,5753 , exp 1229,5774).

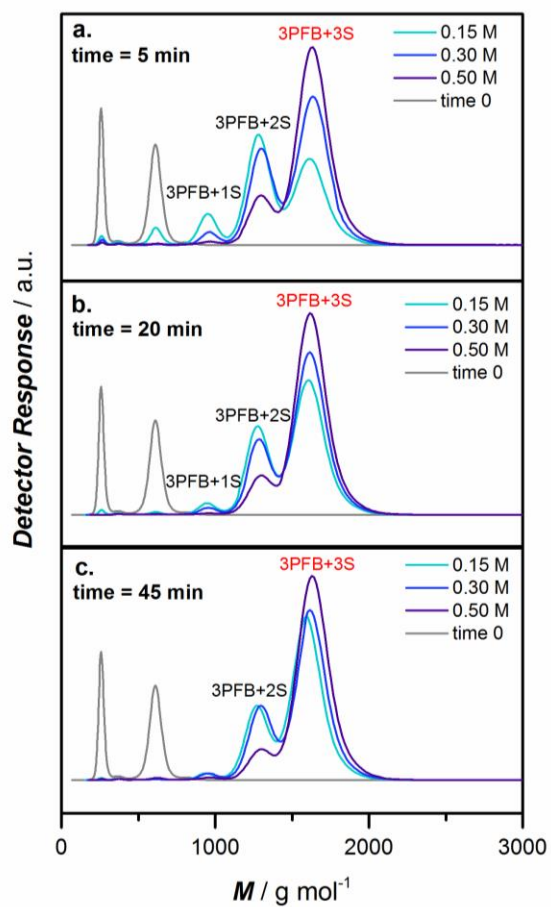


Fig.S6 - SEC traces of different kinetics at specific intervals. Evaluation of the relative abundance of the desired product at: **a.** 5 min, **b.** 20 min, **c.** 45 min. In red the label of the desired product.

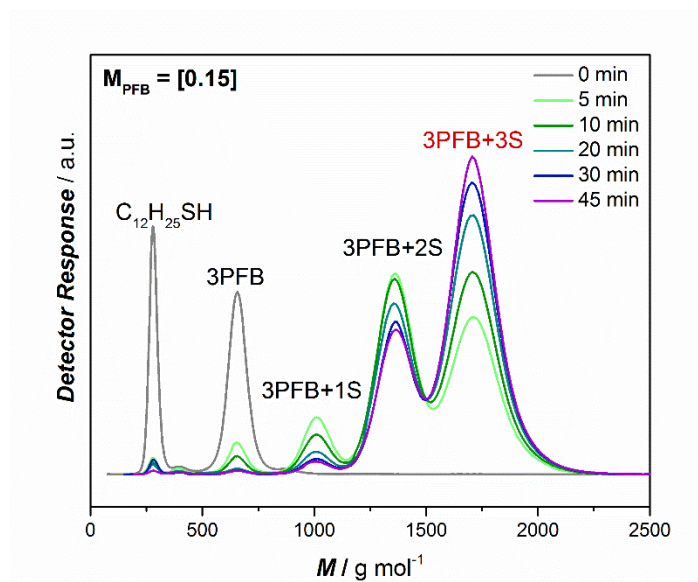


Fig.S7 – SEC traces displaying the evolution of the relative abundance of the desired product along time for a selected concentration ($C_{\text{PFB}} = 0.15 \text{ M}$)

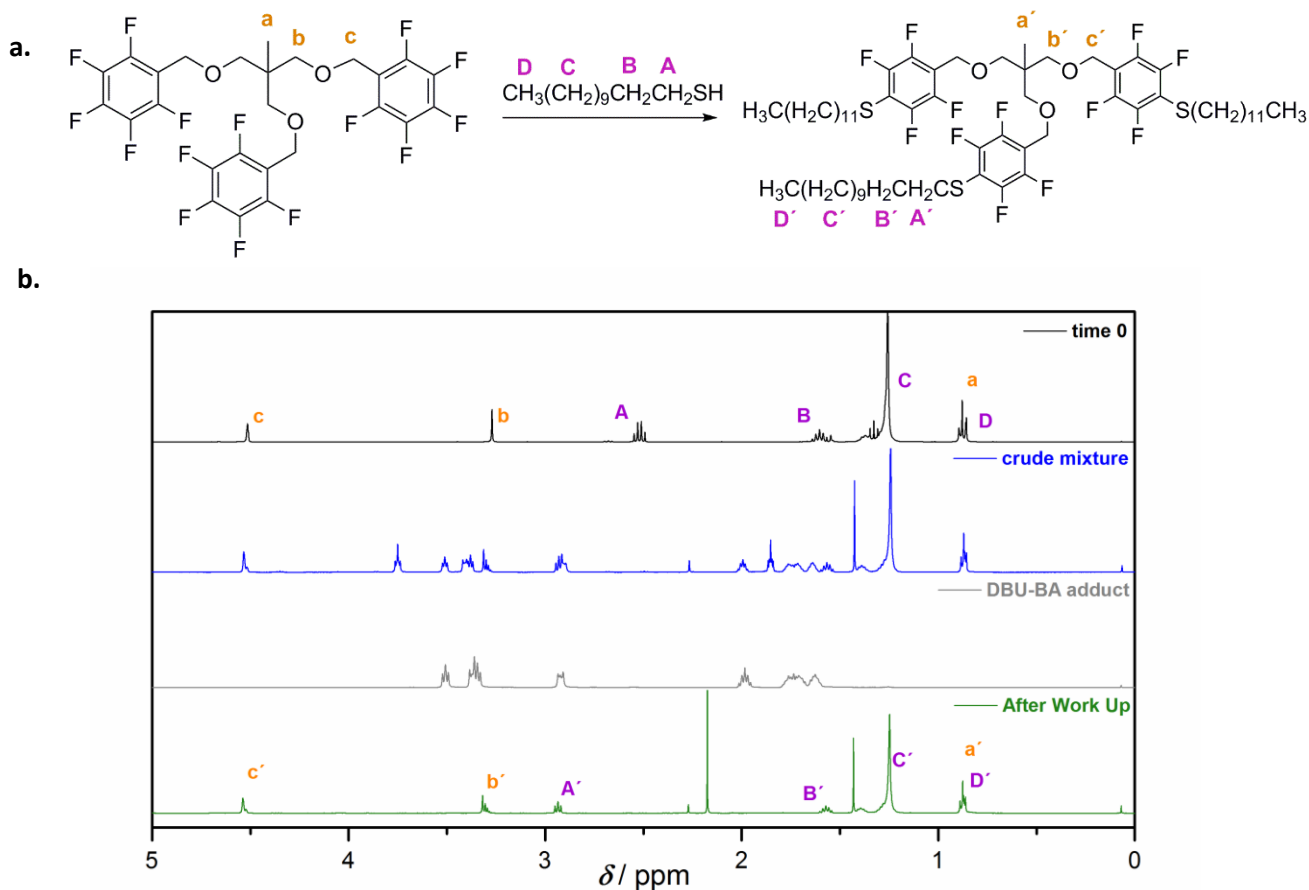


Fig.S8 – **a.** Reaction scheme of the model reaction. **b.** Comparison of $^1\text{H-NMR}$ (400 MHz) spectra for time 0 (black line), crude reaction mixture (blue line), DBU-BA adduct (grey line) and the reaction mixture after work up (green line). It demonstrates the crucial role of the aqueous work up for the detection of the magnetic resonance signals of the adduct.

A.6 General Procedure for Network Formation

As for the model reaction, a stock solution of DBU ($C_{\text{DBU}} = 4 \text{ M}$) and bifunctional thiol ($C_{\text{SH}} = 3 \text{ M}$) were prepared, the amount listed in the procedure refers to the volume of the stock solution.

The 3PFB linker (0.12 mmol, 80 mg, 1 eq.) and DBU (0.36 mmol, 0.054 mL, 3 eq.) was dissolved in a minimum amount of THF (0.2 mL). In the following step, the respective bifunctional thiol (0.18 mmol, 0.060 mL, 1.5 eq.) was added to the aforementioned solution. The reaction mixture instantaneously turns to a gel as a result of the network formation. The freshly formed network is washed with THF to remove the soluble fractions and dried in a vacuum oven overnight at 25 °C.

A comparison of the ATR-IR spectra obtained for the 3PFB linker and the networks is displayed in Fig. S9. The IR spectra can be divided into four main zones. The first zone ranging from $\nu = 4000$ and 2500 cm^{-1} is characteristic for the single bond stretching. Following, one could identify for $\nu = 2500$ to 2000 cm^{-1} the stretching of triple bonds while for $\nu = 2000$ to 1500 cm^{-1} the stretching of double bonds. Eventually, for $\nu < 1500 \text{ cm}^{-1}$ the fingerprint regions starts, where also the C-X bendings appear. After the ligation takes place, the aromatic ring is directly connected to an electron-rich atom (sulphur, S). This will lead to the presence of a resonance structure such as the one reported in Fig. S9b. Combining the two information aforementioned, the two bands underlined by the black boxes at $\nu = 1650 \text{ cm}^{-1}$ and between $\nu = 1000$ - 1200 cm^{-1} refer to the resonance structure **2** and **1** of Fig. S9b, respectively. The second band is also influenced by the C-F and C-O stretching.⁶

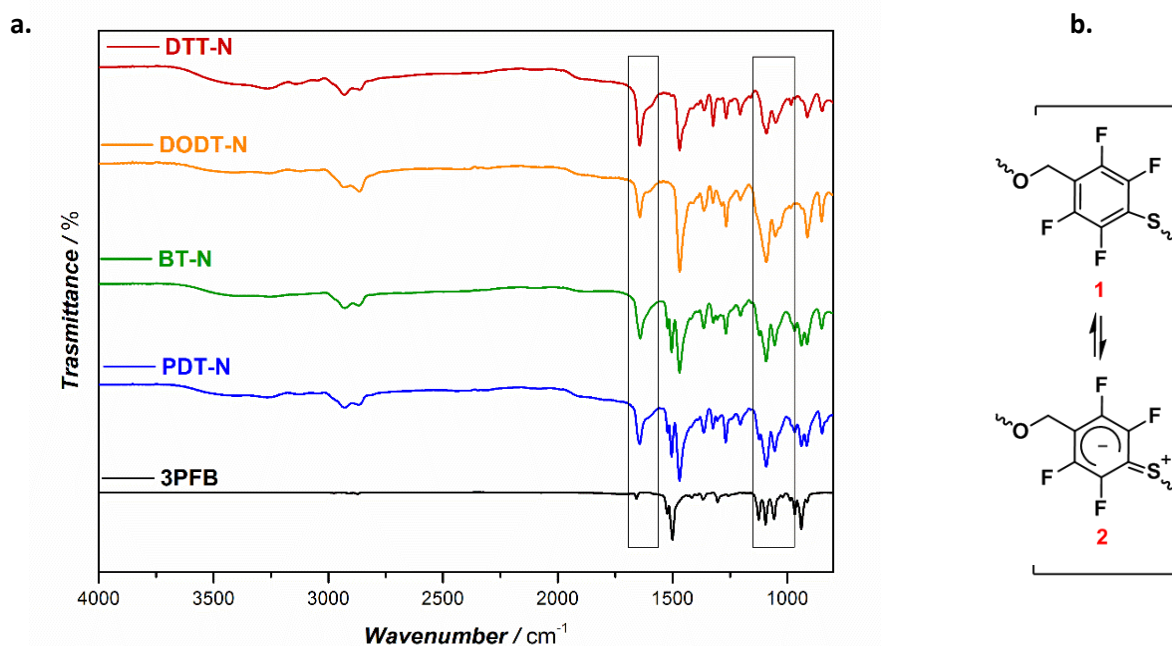


Fig.S9 – a. ATR-IR spectra of the 3PFB linker (black line) and the respective networks obtained with different bifunctional thiol derivatives. b. Resonance structure of the aromatic ring in the product.

^{19}F -NMR spectra are reported for all networks in comparison with 3PFB linker in Fig. S10. 3PFB has already been described in Fig. S3, where the assignment for the magnetic resonances, corresponding to *ortho*- (-143 ppm), *meta*- (-162 ppm) and *para*- (-154 ppm) fluorine atom, are elucidated. On the other hand, the ^{19}F -NMR spectra relative to the network appear to be different from 3PFB, but comparable to the one arising from the product of the “Model Reaction 3+1” reported in the main text. In detail, the magnetic resonance of the *para*-fluorine atom (-154 ppm) disappears and the new *ortho*- and *meta*- resonances are shifted towards lower magnetic field in respect to the pristine ones. This is a consequence of the PTFR itself and of the replacement of one fluorine atom with a sulphur atom. The new magnetic resonance signals appear at -134 and -143 ppm for *ortho*- and *meta*- fluorine respectively.

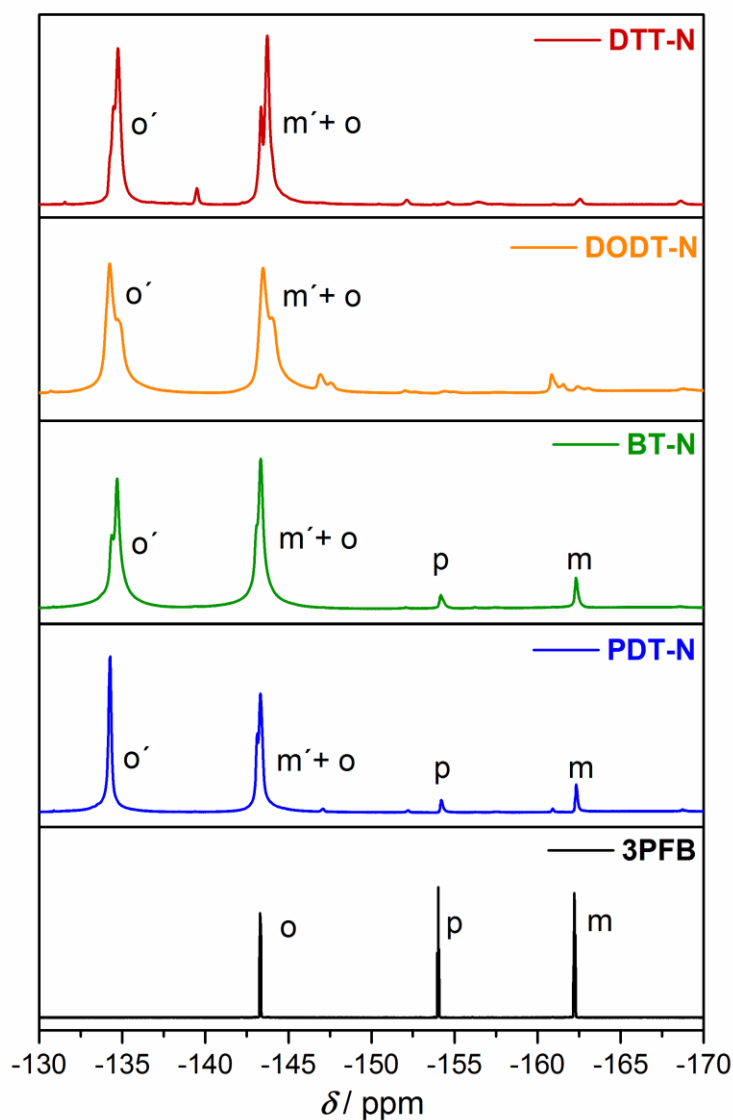


Fig. S10 – ^{19}F -NMR spectra (376 MHz) in CDCl_3 of all synthesized networks compared with the 3PFB linker (black line).

Figure S11 displays the XPS C1s spectra for all the networks obtained compared to the XPS spectrum of the pristine linker 3PFB. In general, the binding energies of the carbon atoms differ according to the atom directly connected to the considered carbon.⁶ This feature allows the discrimination between different carbon bond in the molecule and is used here as a tool to confirm the proposed pathway. In details, starting from the characterization of the 3PFB spectrum, one could identify the peaks specific for the linker core such as C-C, C-O and those for the aromatic moiety with a discrimination between C-F_{o+m} and C-F_{para}. After an extensive literature research, we could find that the mentioned discrimination was already noticed by Chesneau et al. in their system,⁷ but is not visible in system containing the pentafluorophenyl (PFP) group directly connected to an ester moiety.^{8,9} This statement seems to remark the huge influence of the Y group, shown in Scheme 1 of the SI, on the characteristic of the aromatic system. Indeed, additionally to the reported ability to influence the regioselectivity of the reaction (see section A.3), the different Y group seems to be responsible for the slight differences in the chemical shift of the C-F bonds in the XPS spectra.¹⁰ As a consequence, the slight shift between the binding energy values of C-F_{o+m} and C-F_{para} presented here with respect to those reported by Chesneau et al.,⁷ could be justified by the different Y group.¹⁰ Moreover, each group connected to the aromatic ring induce a resonance effect which can be positive or negative (+R and -R) and has to be taken in account during the evaluation of the chemical shift.¹⁰ The latter statement provides an explanation for the different chemical shift between the pristine C-F_{o+m} (288.6 eV) and the same bond after once ligation reaction takes place (C-F_{o'+m'} at 287.8 eV), when a fluorine atom is replaced with a sulphur one. In other words, it is possible to notice that all the spectra show the disappearance of the C-F_{para} peak (light blue curve). Nevertheless, the network systems with DTT-N, DODT-N and BT-N show a small peak of the C-F_{o+m} belonging to an unreacted PFB moiety at 288.6 eV. For what concerns the peaks typical of the ligation reaction, the newly formed C-F_{o'+m'} at 287.8 eV is clearly visible in all network system samples. The same is true for a slight increase of the C-O peak binding energy from 286.5 to 286.2 eV due to the presence and the contribution of the newly formed C-S bonds after the successful application of PFTR for network formation.

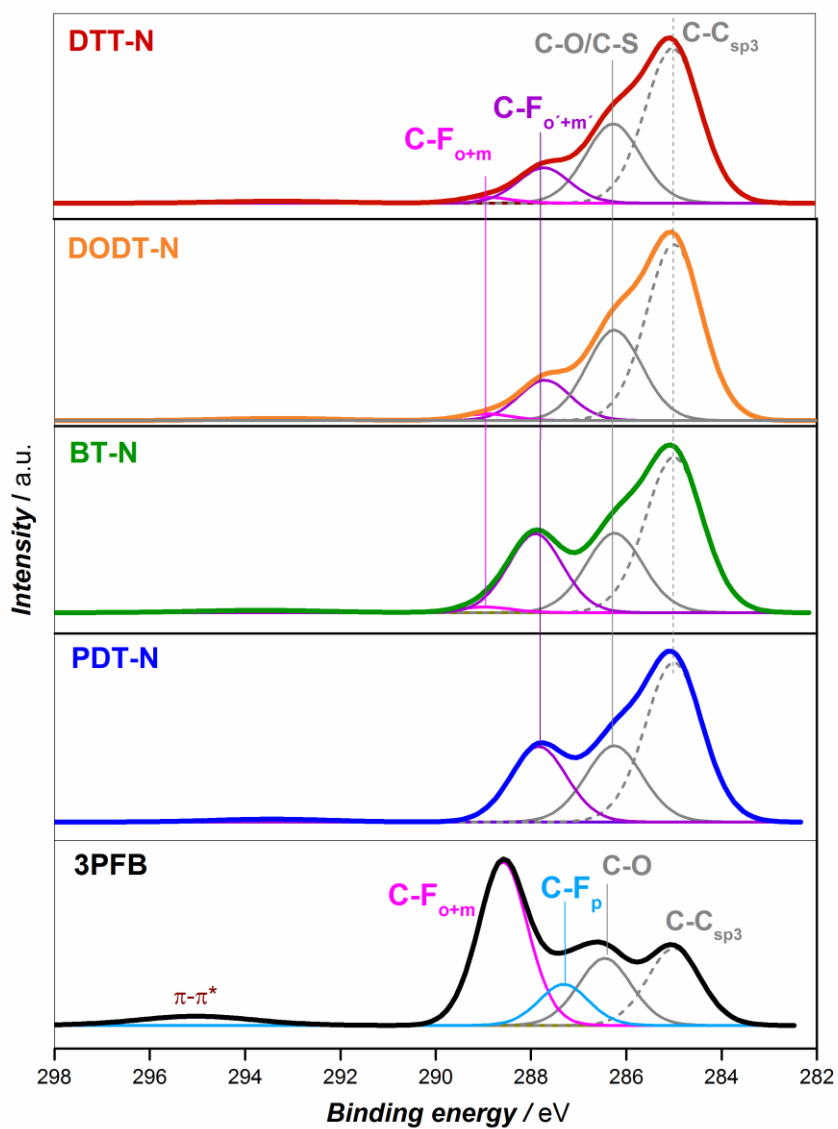


Fig. S11 – Comparative XPS C1s spectra of 3PFB linker (bottom, black line) and the different network synthesized.

Accordingly to the main text, ToF-SIMS analysis was recorded for all network obtained. All images are normalized to the total ion intensity, showing the relative percentage of each detected fragment per pixel. This enables a direct comparison between different samples with similar bulk composition and therefore similar ionization probabilities of secondary ions. Colour scales are identical in images of the same fragment. Here the 3PFB can be identified by the $C_7HOF_5^-$ ion fragment. This fragment shows in all networks lower intensity than in the pure 3PFB linker. The $C_7HSOF_4^-$ is a specific fragment of the ligation network due to the newly formed sulphur bonds. This fragment is not present in the 3PFB but it is clearly visible in all the networks.

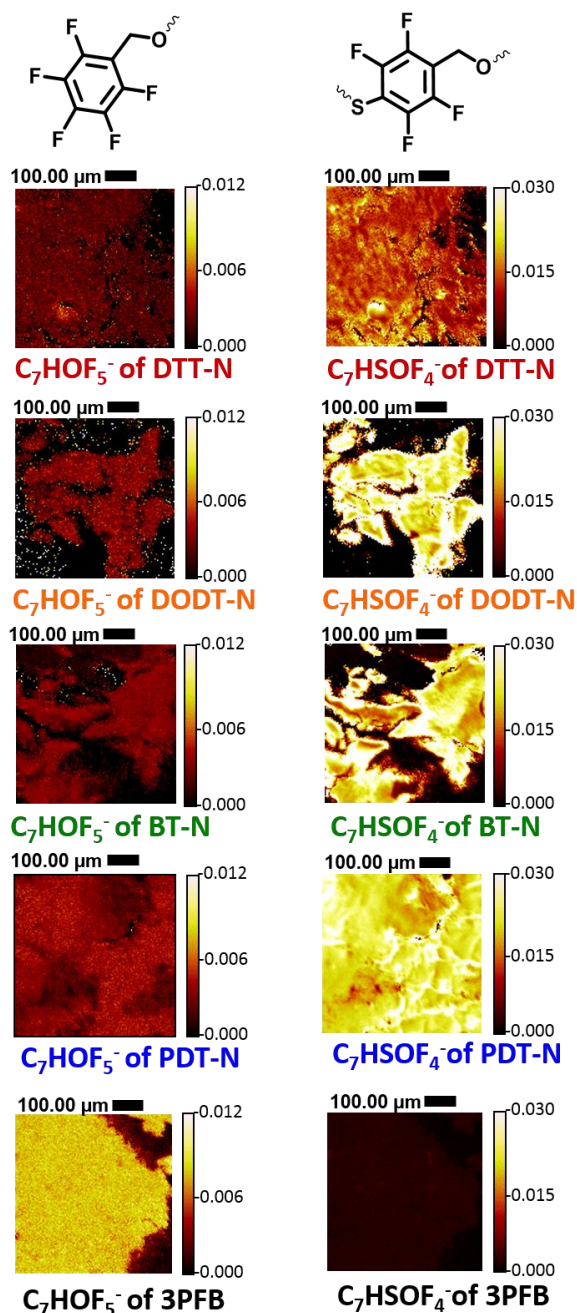


Fig. S12 – Comparison of ToF-SIMS surface image scans of all samples and the 3PFB linker.

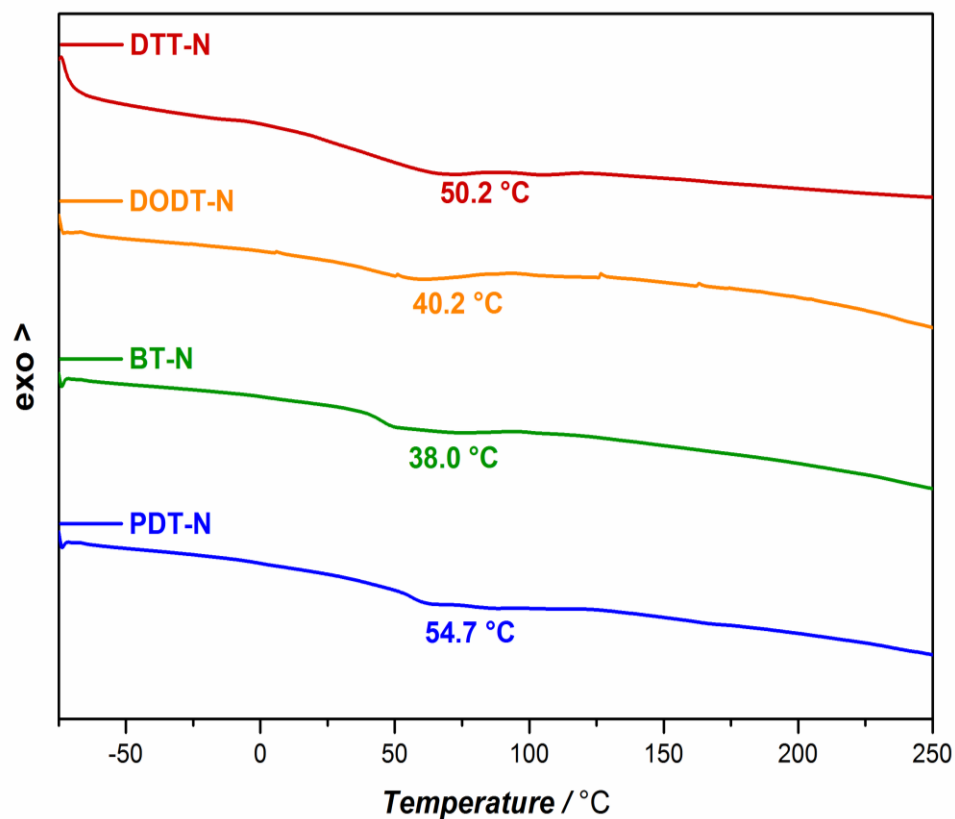


Fig. S13 – Comparative DSC traces of the synthesized networks. The glass transition temperature (T_g) is highlighted. The T_g is reported as temperature detected at the mid-point of the transition.

Table S1 – Results from the swelling test of the obtained network. The absorption ability of the materials in two solvents - THF and ethanol – are shown. The swelling ratio is calculated as the difference of the mass of the sample before and after the swelling test ($\text{wt}\% = [(m_o - m_f) / m_f] * 100$).

Network	Swelling ratio (wt%)	
	THF	Ethanol
DTT-N	31	38
DODT-N	214	64
BT-N	160	35
PDT-N	72	30

References

1. J. H. Scofield, *J. Electron. Spectrosc. Relat. Phenom.*, 1976, **8**, 129-137.
2. S. Tanuma, C. J. Powell and D. R. Penn, *Surf. Interface Anal.*, 1994, **21**, 165-176.
3. L. P. Hammett, *J. Am. Chem. Soc.*, 1937, **59**, 96-103.
4. J. Kvíčala, M. Beneš, O. Paleta and V. Král, *J. Fluorine Chem.*, 2010, **131**, 1327-1337.
5. O. Exner, in *Correlation Analysis in Chemistry: Recent Advances*, eds. N. B. Chapman and J. Shorter, Springer US, Boston, MA, 1978, DOI: 10.1007/978-1-4615-8831-3_10, pp. 439-540.
6. J. Coates, in *Encyclopedia of Analytical Chemistry*, John Wiley & Sons, Ltd, 2006, DOI: 10.1002/9780470027318.a5606.
7. F. Chesneau, H. Hamoudi, B. Schüpbach, A. Terfort and M. Zharnikov, *The Journal of Physical Chemistry C*, 2011, **115**, 4773-4782.
8. L. Duque, B. Menges, S. Borros and R. Förch, *Biomacromolecules*, 2010, **11**, 2818-2823.
9. K. A. Gunay, N. Schuwer and H.-A. Klok, *Polym. Chem.*, 2012, **3**, 2186-2192.
10. B. C. Trudell and S. J. W. Price, *Can. J. Chem.*, 1978, **56**, 538-542.